

Left Ventricular Assist Device Flow Pattern Analysis Using a Novel Model Incorporating Left Ventricular Pulsatility

Jonathan Grinstein^{a*}, Ryo Torii^b, Christos V. Bourantas^c and Hector M. Garcia-Garcia^d

^a Department of Medicine, Section of Cardiology, University of Chicago, Chicago, Illinois

^b Department of Mechanical Engineering, University College of London, London, United Kingdom

^c Barts Heart Centre, Department of Cardiology, London, United Kingdom

^d MedStar Cardiovascular Research Network, Washington, DC.

**Corresponding author*

Jonathan Grinstein, MD, FACC

Department of Medicine, Section of Cardiology, Advanced Heart Failure, Transplant and Mechanical Circulatory Support, University of Chicago,

5841 S Maryland Ave, A621-MC2016, Chicago, IL 60637.

Email: jgrinstein@medicine.bsd.uchicago.edu

Disclosure

J.G. is a consultant for NuPulse CV and Medtronic Inc. All authors have a patent pending on this CFD model. There are no other relevant conflicts of interest for any author.

ABSTRACT

Our current understanding of flow through the circuit of left ventricular assist device (LVAD), left ventricle and ascending aorta remains incompletely understood. Computational fluid dynamics (CFD), which allow for analysis of flow in the cardiovascular system, have been used for this purpose, although current simulation models have failed to fully incorporate the interplay between the pulsatile left ventricle and continuous-flow generated by the LVAD. Flow through the LVAD is dependent on the interaction between device and patient specific factors with suboptimal flow patterns evoking increased risk of LVAD-related complications. CFD can be used to analyze how different pump and patient factors affect flow patterns in the left ventricle and the aorta.

CFD simulations were carried out on a patient with a HeartMate II. Simulations were also conducted for theoretical scenarios substituting HeartWare HVAD, HeartMate 3 (HM3) in continuous mode and HM3 with Artificial Pulse. An anatomical model of the patient was reconstructed from computed tomography (CT) images, and the LVAD outflow was used as the inflow boundary condition. The LVAD outflow was calculated separately using a lumped-parameter-model (LPM) of the systemic circulation, which was calibrated to the patient based on the patient-specific ventricular volume change reconstructed from 4 dimensional CT and pulmonary capillary wedge pressure tracings. The LVADs were implemented in the LPM via published pressure head vs. flow (H-Q) curves. In order to quantify the flushing effect, virtual contrast agent was released in the ascending aorta and its flushing over the cycles was quantified. Shear stress acting on the aortic endothelium and shear rate in the blood stream were also quantified as indicators of normal/abnormal blood flow, especially the latter being a biomarker of platelet activation and hemolysis.

Under standard operating conditions of the LVADs (9000 RPM for HMII, 5500 RPM for HM3 and 2600 RPM for HVAD), the cardiac outputs were 5.92 L/min, 6.14 L/min and 6.90 L/min, respectively. The velocity of blood flow in the outflow cannula was higher in the HVAD than in the two HeartMate pumps with a cycle average (range) of 0.72 m/s (0.57-0.93 m/s), 0.70 m/s (0.64-0.77 m/s) and 1.61 m/s (1.21-1.92 m/s) for HMII, HM3 and HVAD, respectively. Artificial pulse increased the peak flow rate to 9.84 L/min for the HM3 but the overall cardiac output was 5.96 L/min, which was similar to the continuous mode. Artificial pulse markedly decreased blood stagnation in the ascending aorta; after 6 cardiac cycles, 43% of the blood was flushed out from the ascending aorta under the continuous operation mode while 61% was flushed under artificial pulse. Shear stress in the aortic arch and shear rate in the ascending aorta were higher with the HVAD compared to the HMII and HM3, respectively (Shear Stress: 2.18 vs. 1.33 vs. 1.33 Pa, Shear Rate: 28.5 vs. 13.2 vs. 11.6 s⁻¹).

Pump-specific factors such as LVAD type and programmed flow algorithms lead to unique flow patterns which influence blood stagnation, shear stress and platelet activation. The pump-patient interaction can be studied using a novel CFD model to better understand and potentially mitigate the risk of downstream LVAD complications.

INTRODUCTION

The left ventricular assist device (LVAD) is a durable mechanical pump that provides constant unloading of the LV in patients with advanced heart failure. Since 2006, over 17,000 patients have been implanted with an FDA-approved continuous-flow LVAD with a current implant rate of greater than 2,500 new LVADs per year (1). Actuarial survival following LVAD implant is 81% at 1 year and 70% at 2 years (1). Despite the survival benefit, adverse events remain common with up to 60% of patients experiencing an adverse event within 6 months and 80% of patients experiencing a complication within 2 years of implantation (2).

Our current understanding of flow through an LVAD is largely based on ex vivo and in vivo modeling using a combination of artificial circuits, computer simulations and animal models (3-8). Few studies have examined the flow patterns in humans supported with LVADs. Recently, computational fluid dynamics (CFD) has emerged as a promising technique to further analyze flow patterns in the cardiovascular system. CFD has been applied to non-invasively quantify pressure changes and flow within coronary arteries, based on cardiac computed tomography (CT), as well as other vascular beds (9,10). More recently, CFD has been used to study in patients with advanced heart failure the hemodynamic impact of a possible LVAD implant (11). Models have also assessed the impact of inflow and outflow cannula angulation as well as aortic valve opening on flow patterns, shear stress and thrombotic potential (12-15).

Although the current generation of LVADs deliver continuous-flow, the net flow that is transmitted to the patient is still pulsatile as a result of a constantly changing pressure gradient across the LVAD during different stages of the cardiac cycle, irrespective of the presence of aortic valve opening (16,17). Previous CFD models investigating flow patterns through the LVAD have not fully incorporated the interaction between the pulsatile LV and continuous-flow generated by the LVAD. Here we present the first known model which incorporates a complete hemodynamic and structural assessment of the pump-patient interaction during each stage of the cardiac cycle. Utilizing this model, the interplay between LVAD anatomic positioning, flow and patient outcomes can be better studied with the aim at mitigating adverse events for advanced heart failure patients supported by an LVAD.

METHODS

Patient selection

From our LVAD cohort of patients at Medstar Washington Hospital Center, we identified a patient with concurrent contrast four-dimensional CT images and a complete hemodynamic assessment by right heart catheterization. This patient received HeartMate II (HMII, Abbott, Chicago IL) in 2015. This research project has received IRB approval.

Computational Fluid Dynamic Modeling

A computational model framework to achieve personalised performance prediction of the cardiovascular system including LVAD was developed. The overall concept was centred around a computational model of the flow circuit, from left atrium and ventricle, LVAD and

aorta. The model is personalised for each patient by reflecting information acquired through routine clinical measurements, hemodynamic measurements and gated imaging. In the current form, detailed anatomical information was introduced in the model by means of high-resolution, four-dimensional CT images together with pulmonary capillary wedge pressure tracings from right heart catheterization. Additional patient specific variables incorporated to calibrate the model included blood pressure and heart rate as well as haematocrit and blood protein level (total and albumin) to estimate patient-specific non-Newtonian blood viscosity following Walburn and Schneck (18). Cardiac elastance and vascular resistance and compliance in the large arteries were modelled according to published values (19,20).

The actual model is constructed in two steps as shown in **Figure 1**: model of circulation using (1) electrical circuit analogy and (2) three-dimensional (3D) CFD. The former allows estimation of physiological response to the LVAD operation, including different modes of operation such as artificial pulsing, and the latter allows detailed depiction of flow patterns and hemodynamic indicators such as wall shear stress to evaluate the performance of the LVAD in terms of its potential impact on the physiologic system. In the electrical circuit analogue model, vascular resistance and compliance are represented by the electrical resistance and capacitance; each of LVAD and ventricle are represented by a power source. The resistance, capacitance and other parameters of each component were calibrated such that the model performance (e.g. in terms of left atrial pressure) approximated well the measured values (e.g. pulmonary capillary wedge pressure for the left atrial pressure) following published procedures (20). Once the model parameters were determined, LVAD

operation modes were varied to obtain the flow and pressure in the aorta as well as LV, which were then fed into the 3D model.

The 3D model computation was carried out by solving equations of fluid motion (Navier-Stokes equations) and mass conservation in the spatial domain of the aorta. *The 3D anatomical model was reconstructed from high-resolution CT (typical resolution of 0.54 mm/pixel) using Simpleware ScanIP (Synopsys, Inc. CA USA). A commercial CFD package ANSYS CFX was used for blood flow simulations. The blood was assumed to have homogenous density, 1060 kg/m³, and Walburn-Schneck model was used to model the shear-thinning behaviour of the blood viscosity that also reflects patient-specific viscosity using total protein and albumin levels [g/dL] of the patient's blood (18). As described earlier, the waveform of the volumetric blood flow from the LVAD to the aorta was prescribed at the inlet of LVAD outflow cannula and typical flow split in the head vessels (10% of the cardiac output to brachiocephalic, 5% to left common carotid and 5% to left subclavian arteries was specified as the outflow boundary conditions. For the remaining outlets, outflow conditions were set using zero relative pressure. The arterial and cannula wall were approximated as rigid wall and no-slip boundary conditions were applied.*

The combination of 3D CFD model and the LPM allows not only visualization and quantification of the pattern of flow under various LVAD operating modes but also realization of hypothetical scenarios related to outflow cannula geometry (diameter) or LVAD flow control algorithms in order to identify the best-performing configuration of the LVAD for an optimal circulatory function.

Variation of LVAD type and Flow Algorithm

Based on the anatomical model of the patient with a HMII (Figure 2A), simulations were carried out for hypothetical scenarios substituting HeartWare HVAD (Medtronic, Minneapolis, MN) (Figure 2B) with and without the Lavare cycle, HeartMate 3 (HM3, Abbott, Chicago IL) in continuous mode (Figure 2C) and HM3 with Artificial Pulse (Figure 2D). The anatomical model of the patient, reconstructed from CT images as described earlier, was kept unchanged for HM3 whereas the outflow cannula diameter was reduced from 14 mm to 10 mm for the HVAD case. For all the cases, the LVAD outflow was calculated first using a lumped-parameter model (LPM) of the systemic circulation including LVAD and used as the inflow boundary condition to the outflow cannula. The LPM of the systemic circulation was calibrated to the patient based on the patient-specific ventricular volume change reconstructed from four-dimensional CT, aortic pressure and pulmonary capillary wedge pressure tracings. The LVADs were implemented in the LPM via published H-Q curves in the continuous mode at 9000 RPM, 5500 RPM and 2600 RPM for HMII, HM3 and HVAD, respectively (21,22). The operational condition for HMII is for the actual patient and those for HM3 and HVAD are standard for producing 5.5 L/min flow against 60 mmHg pump head.

Additionally to the continuous mode of operation, two commercially-available pulsatile flow conditions were tested: Artificial pulse for HM3 and Lavare cycle for HVAD. Artificial pulse was incorporated by controlling the operating condition ± 2000 RPM for short duration (0.15 s reduction and 0.2 s increase) every 2 seconds (22). Lavare cycle was

incorporated by controlling the operation condition ± 200 RPM for moderate duration (2 s reduction and 1 s increase) every 60 seconds (23). Further, concepts of co-pulsation and counter-pulsation were tested to investigate the impact of these conditions on the flow patterns. Here, the rotational speed was increased by 200 RPM during systole (0-30% of the cycle) and diastole (50%-80% of the cycle), respectively.

In order to quantify the flushing effect in the aorta, virtual contrast agent was released in the ascending aorta and its flushing over the cycles was quantified. Transport of the contrast agent in the blood stream was calculated by solving an equation for mass transport, additionally to the equations of the flow motion in ANSYS CFX. Initially, the entire aorta as well as the outflow cannula was filled with conventional level of X-ray contrast, 700 mg/mL, and the contrast was carried away from the domain by the flow through the aorta. Shear stress acting on the aortic endothelium and shear rate in the blood stream were also quantified as indicators of normal/abnormal blood flow. Calculation of the two parameters was based on the spatial gradient of blood flow velocity, coming out from the process of CFD simulation. Shear stress is defined on the blood-facing side of the endothelial layer (i.e. lumen-wall border) and calculated as a product of local velocity gradient by blood viscosity. This has been widely used as an indicator of normal/abnormal hemodynamic stimuli to the arterial wall (24). Shear rate is defined as the velocity gradient between adjacent blood flow streamlines (Figure 2). It allows quantitative representation of flow disturbance and has been referred as a biomarker of platelet activation and hemolysis (25). Throughout the simulations, the aortic valve was kept closed, which reflects the clinical observation in this specific case.

RESULTS

Under standard operation conditions of the LVADs (9000 RPM for HMII, 5500 RPM for HM3 and 2600 RPM for HVAD), the mean flow rates were 5.81 L/min, 5.83 L/min and 6.85 L/min, for HMII, HM3 and HVAD, respectively. The velocity of blood flow in the outflow cannula was higher in the HVAD than in the two HeartMate pumps with a cycle average (range) of 0.92 m/s (range 0.78-1.19 m/s), 0.91 m/s (range 0.86-1.00 m/s) and 1.70 m/s (range 1.52-2.05 m/s) for HMII, HM3 and HVAD, respectively. Artificial pulse increased the peak flow rate to 9.80 L/min for the HM3 but the overall mean flow rate was 5.65 L/min, which was similar to the continuous mode (**Figure 3**). The flushing of blood from the ascending aorta was better for HVAD cases, with approximately 28% of blood remaining after 6 seconds. For the HM3, the addition of the artificial pulse markedly decreased blood stagnation in the ascending aorta; after 6 seconds (7.5 cardiac cycles), 49% of the blood was flushed out from the ascending aorta under the continuous operation mode while 60% was flushed under artificial pulse (**Figure 4**).

Shear stress was greater with the HVAD when compared to the HMII or HM3. In the aortic arch and cerebral head vessels, a 64% increase in shear stress was noted with the HVAD compared to the HM3 in continuous mode (2.18 vs. 1.33 Pa). By comparison, the HVAD led to a 157% increase in shear stress in the ascending aorta (0.507 vs. 0.197 Pa). The addition of the artificial pulse to the HM3 flow algorithm led to a 48% increase in shear stress (0.291 vs 0.197 Pa) throughout the ascending aorta (**Figure 5**). On the contrary, the differences of shear stress due to the mode of operations, i.e. continuous mode vs non-continuous modes,

was small with the maximum difference of 6% in the ascending aorta between continuous vs Artificial Pulse of HM3 (1.49 Pa vs 1.58 Pa).

Shear rate was elevated throughout the entirety of the thoracic aorta, particularly in the outflow cannula, in the HVAD model compared to the HM3 in continuous mode (**Figure 6**). Shear rate in the outflow cannula of HVAD cases are 325% higher than the cases with HM2 and HM3 (approximately 500 vs 155 s⁻¹). The blood volume exposed to shear rate 1000 s⁻¹ is also markedly higher for LVAD cases, approximately 2 cm³ (1% of total aortic volume) is exposed to the high shear rate whereas such volume is 1/10 in the other cases.

DISCUSSION

The main findings of our study are: 1. This is the first model using actual patient information to simulate flow conditions in an LVAD patient accounting for pulsatility; 2. Three existing LVADs scenarios were compared in terms of cardiac output, flow velocity, blood stagnation and shear stress; 3. Programmable flow algorithms applied to the different LVADs influence blood stagnation in the aortic root and shear stress.

By combining high fidelity imaging in the form of gated cardiac CT together with patient-derived hemodynamic and physiological variables, CFD provides a unique ability to better assess flow through the LVAD and its associated clinical implications. In addition to flow pattern analysis, CFD allows assessment of blood stagnation, shear rate and shear stress, known risk factors for platelet activation, thrombin formation and aortic insufficiency, which account for a large component of LVAD-related morbidity (12,14,26).

It is largely believed that much of the morbidity following LVAD implant is interrelated to the relationship of the LVAD (anatomic position, flow currents, hemocompatibility of the pump components) with the patient, the so-called pump-patient interaction. High shear rates have been associated with von Willebrand factor unfolding and bleeding whereas low shear rates have been associated with thrombus formation (27-29). High shear stress leads to platelet activation whereas low shear stress in the ascending aorta has been implicated in aortic insufficiency progression in LVAD patients (30-33). Suboptimal positioning and angulation of the outflow cannula is associated with blood stagnation in the aortic root and higher wall shear stress in the ascending aorta (13). Similarly, a more acute outflow cannula anastomosis is associated with less thrombogenic potential (14). Misalignment of the inflow cannula impairs LV unloading, and is associated with increased heart failure admissions (34). Increased angulation of the inflow cannula has similarly been linked to ventricular tachycardia, hemolysis and thrombosis (12,35,36).

The latest centrifugal flow LVADs, the Heartware HVAD and the HeartMate 3 provide cyclical flow patterns where the LVAD rotor speed is decreased then increased by a set amplitude and at a set interval which is unique to each pump. These flow algorithms were introduced in an effort to mitigate thrombus formation. In theory, there are several mechanisms whereby cyclical variation in rotor speed may decrease thrombus formation potential including washing out of the rotor, aortic valve and aortic root washout, promoting intermittent aortic valve opening and promoting more vascular recoil and pulsatility. Here, our boundary conditions assumed that the aortic valve was closed the entire time and the aortic vasculature was fixed and thus the effects of the flow algorithms are attributable to the flushing effects of blood via the outflow cannula. Further modeling

taking into account aortic valve opening and vascular recoil may add additional mechanisms by which these flow algorithms may be beneficial.

The flow pattern, termed the Lavare Cycle, for the HVAD is conditional and the decision to turn off or on the cycle is dependent on the user. The flow pattern for the HM3, termed the Artificial Pulse, is currently an obligatory setting. The Heartmate II axial flow LVAD, conversely only provides a fixed speed without the option for pre-programmed cyclical flow pattern. By providing cyclic de-escalation followed by escalation of the rotational speed of the pump, speed variation algorithms allow for washout of areas of blood stagnation in the pump casing and rotor (37). Here we show that the artificial pulse – without increasing overall cardiac output – also decreases blood stagnation in the aortic root, another potential source of thrombus formation, particularly in patients with closed aortic valves. At the same time, Lavare Cycle was not effective in terms of blood washout, in comparison to the continuous operation mode of HVAD. The artificial pulse did increase ascending aortic root wall shear stress which may partially explain the aortic insufficiency prevalence with this pump type. Shear rate was most elevated in the HVAD model, particularly in the aortic arch and head vessels. This may contributed to the heightened stroke rate observed with the HVAD, even after accounting for blood pressure as a modifiable risk factor (38). As the current and future generation of LVADs become more customizable, our model will also allow users to choose the ideal flow pattern to minimize stagnation and shear stress while at the same time maximize aortic valve opening and unloading.

Our model is unique in that it fully integrates the pulsatile flow contributions from the LV using a combination of measured intracardiac hemodynamics together with assumptions about the boundary conditions and LV contractility from gated computed tomography in an actual patient supported with an LVAD. Recent models using CFD to explore flow through the LVAD have been less physiologic, as they either did not incorporate the left ventricle contribution to flow or were developed as “virtual surgeries” where an LVAD was later added to the anatomy of a patient who was not originally supported with an LVAD (12,14,15). Previous models that have attempted to incorporate LV pulsatility have focused on the outflow cannula and aorta and have used indirect assumptions about pressure variation in the ventricle without incorporating patient-specific intracardiac hemodynamics (13,26). Our model is the first fully pulsatile model that integrates systolic and diastolic pressure variation within the LV and also include the entire left ventricle, LVAD system (inflow cannula, pump and outflow cannula) as well as the aorta. Given the dynamic nature of our model, it allows for more accurate assessment of periodic perturbations in flow patterns such as transient inflow cannula obstruction during different phases of the cardiac cycle.

LIMITATIONS

The modeling and analysis were developed based on the anatomic and physiologic data from a single patient previously implanted with a HMII. Although patient specific data was used to calibrate the model to make the flow conditions as physiologic as possible, there remain several unmeasured variables including properties related to vessel and chamber

elastance and compliance that could not be fully accounted for in the model and thus had to be estimated based on previously published equations. Furthermore, the modeling assumed that the mitral valve was competent and that the aortic valve was closed throughout the cardiac cycle. Future versions of the model will need to address valve regurgitation to be more clinically applicable. Our study should be interpreted as hypothesis generating in its current form. Further validation of the model using prospective data collection and verification of flow patterns using direct Doppler imaging is needed. A prospective analysis is needed to further optimize the modelling to allow for more incorporation of more patient-specific information.

CONCLUSIONS

Pump-specific factors such as the LVAD type implanted and programmed flow algorithms lead to unique flow patterns. In particular, the artificial pulse of the HeartMate 3 may lead to more optimal aorta washout and less thrombogenic potential in the aortic root secondary to blood stagnation. The HVAD was associated with increased shear rate, particularly in the aortic arch and head vessels and this may partially contribute to the increased residual stroke rate with this pump, even after accounting for blood pressure management. Perturbations in the pump-patient interactions using this novel CFD model that fully incorporates the pulsatile left ventricle together with continuous flow component from the LVAD will allow us to better understand and potentially mitigate the risk of downstream LVAD complications.

ACKNOWLEDGEMENTS

Jonathan Grinstein is a consultant for NuPulse CV. All authors have a patent pending on this CFD model. There is no funding source for this work. There are no other relevant conflicts of interest for any author.

REFERENCES

1. Kirklin JK, Pagani FD, Kormos RL et al. Eighth annual INTERMACS report: Special focus on framing the impact of adverse events. *J Heart Lung Transplant* 2017;36:1080-1086.
2. Wever-Pinzon O, Drakos SG, Kfoury AG et al. Morbidity and mortality in heart transplant candidates supported with mechanical circulatory support: is reappraisal of the current United network for organ sharing thoracic organ allocation policy justified? *Circulation* 2013;127:452-62.
3. Sénage T, Février D, Michel M et al. A mock circulatory system to assess the performance of continuous-flow left ventricular assist devices (LVADs): does axial flow unload better than centrifugal LVAD? *ASAIO J* 2014;60:140-7.
4. Stonehouse A, Cook M, Woodard J. VentrAssist left ventricular assist systems long-term in vitro reliability. *Artif Organs* 2009;33:860-4.
5. Timms D, Hayne M, McNeil K, Galbraith A. A complete mock circulation loop for the evaluation of left, right, and biventricular assist devices. *Artif Organs* 2005;29:564-72.
6. McCormick M, Nordsletten DA, Kay D, Smith NP. Simulating left ventricular fluid–solid mechanics through the cardiac cycle under LVAD support. *Journal of Computational Physics* 2013;244:80-96.
7. McCormick M, Nordsletten D, Lamata P, Smith NP. Computational analysis of the importance of flow synchrony for cardiac ventricular assist devices. *Comput Biol Med* 2014;49:83-94.
8. Monreal G, Sherwood LC, Sobieski MA, Giridharan GA, Slaughter MS, Koenig SC. Large animal models for left ventricular assist device research and development. *ASAIO J* 2014;60:2-8.
9. Taylor CA, Fonte TA, Min JK. Computational fluid dynamics applied to cardiac computed tomography for noninvasive quantification of fractional flow reserve: scientific basis. *J Am Coll Cardiol* 2013;61:2233-41.
10. Morris PD, Narracott A, von Tengg-Kobligk H et al. Computational fluid dynamics modelling in cardiovascular medicine. *Heart* 2016;102:18-28.
11. Capoccia M, Marconi S, Singh SA, Pisanelli DM, De Lazzari C. Simulation as a preoperative planning approach in advanced heart failure patients. A retrospective clinical analysis. *Biomed Eng Online* 2018;17:52.
12. Chivukula VK, Beckman JA, Prisco AR et al. Left Ventricular Assist Device Inflow Cannula Angle and Thrombosis Risk. *Circ Heart Fail* 2018;11:e004325.

13. Callington A, Long Q, Mohite P, Simon A, Mittal TK. Computational fluid dynamic study of hemodynamic effects on aortic root blood flow of systematically varied left ventricular assist device graft anastomosis design. *J Thorac Cardiovasc Surg* 2015;150:696-704.
14. Aliseda A, Chivukula VK, McGah P et al. LVAD Outflow Graft Angle and Thrombosis Risk. *ASAIO J* 2017;63:14-23.
15. Mahr C, Chivukula VK, McGah P et al. Intermittent Aortic Valve Opening and Risk of Thrombosis in Ventricular Assist Device Patients. *ASAIO J* 2017;63:425-432.
16. Burkhoff D, Sayer G, Doshi D, Uriel N. Hemodynamics of Mechanical Circulatory Support. *J Am Coll Cardiol* 2015;66:2663-2674.
17. Mancini D, Colombo PC. Left Ventricular Assist Devices: A Rapidly Evolving Alternative to Transplant. *J Am Coll Cardiol* 2015;65:2542-55.
18. Walburn FJ, Schneck DJ. A constitutive equation for whole human blood. *Biorheology* 1976;13:201-10.
19. Kim HJ, Vignon-Clementel IE, Coogan JS, Figueroa CA, Jansen KE, Taylor CA. Patient-specific modeling of blood flow and pressure in human coronary arteries. *Ann Biomed Eng* 2010;38:3195-209.
20. Pirola S, Cheng Z, Jarral OA et al. On the choice of outlet boundary conditions for patient-specific analysis of aortic flow using computational fluid dynamics. *J Biomech* 2017;60:15-21.
21. Noor MR, Ho CH, Parker KH, Simon AR, Banner NR, Bowles CT. Investigation of the Characteristics of HeartWare HVAD and Thoratec HeartMate II Under Steady and Pulsatile Flow Conditions. *Artif Organs* 2016;40:549-60.
22. HeartMate 3 Left Ventricular Assist System Instruction for Use. Pleasanton CA: Thoratec Corporation, 2017.
23. HVAD System Instructions for Use. Framingham MA: HeartWare, Inc., 2017.
24. Thondapu V, Bourantas CV, Foin N, Jang IK, Serruys PW, Barlis P. Biomechanical stress in coronary atherosclerosis: emerging insights from computational modelling. *Eur Heart J* 2017;38:81-92.
25. Ng J, Bourantas CV, Torii R et al. Local Hemodynamic Forces After Stenting: Implications on Restenosis and Thrombosis. *Arterioscler Thromb Vasc Biol* 2017;37:2231-2242.
26. Karmonik C, Partovi S, Loebe M et al. Computational fluid dynamics in patients with continuous-flow left ventricular assist device support show hemodynamic alterations in the ascending aorta. *J Thorac Cardiovasc Surg* 2014;147:1326-1333.e1.
27. Hubbell JA, McIntire LV. Visualization and analysis of mural thrombogenesis on collagen, polyurethane and nylon. *Biomaterials* 1986;7:354-63.
28. Nanna JC, Navitsky MA, Topper SR, Deutsch S, Manning KB. A fluid dynamics study in a 50 cc pulsatile ventricular assist device: influence of heart rate variability. *J Biomech Eng* 2011;133:101002.
29. Schneider SW, Nuschele S, Wixforth A et al. Shear-induced unfolding triggers adhesion of von Willebrand factor fibers. *Proc Natl Acad Sci U S A* 2007;104:7899-903.

30. Brown CH, Leverett LB, Lewis CW, Alfrey CP, Hellums JD. Morphological, biochemical, and functional changes in human platelets subjected to shear stress. *J Lab Clin Med* 1975;86:462-71.
31. Anderson GH, Hellums JD, Moake J, Alfrey CP. Platelet response to shear stress: changes in serotonin uptake, serotonin release, and ADP induced aggregation. *Thromb Res* 1978;13:1039-47.
32. May-Newman K, Enriquez-Almaguer L, Posuwattanakul P, Dembitsky W. Biomechanics of the aortic valve in the continuous flow VAD-assisted heart. *ASAIO J* 2010;56:301-8.
33. Martina JR, Schipper ME, de Jonge N et al. Analysis of aortic valve commissural fusion after support with continuous-flow left ventricular assist device. *Interact Cardiovasc Thorac Surg* 2013;17:616-24.
34. Imamura T, Nguyen A, Chung B et al. Association of Inflow Cannula Position with Left Ventricular Unloading and Clinical Outcomes in Patients with HeartMate II Left Ventricular Assist Device. *ASAIO J* 2018.
35. Alvarez PA, Kassi M, Loebe M, Estep J, Bhimaraj A, Chang SM. A Quantitative Assessment of Left Ventricular Assist Device Inflow Cannula Position with Contrast Enhanced Gated Cardiac Multislice Computed Tomography and Its Clinical Correlation. *ISHLT 33rd Annual Meeting & Scientific Sessions, Montreal, Canada - April 24-27, 2013* 2013;32:S229.
36. Bhamra JK, Bansal A. Left Ventricular Assist Device Inflow Cannula Position May Contribute to the Development of HeartMate II Left Ventricular Assist Device Pump Thrombosis. *Ochsner J* 2018;18:131-135.
37. Bourque K, Cotter C, Dague C et al. Design Rationale and Preclinical Evaluation of the HeartMate 3 Left Ventricular Assist System for Hemocompatibility. *ASAIO J* 2016;62:375-83.
38. Milano CA, Rogers JG, Tatroles AJ et al. HVAD: The ENDURANCE Supplemental Trial. *JACC Heart Fail* 2018;6:792-802.

Electric circuit (lumped parameter) model

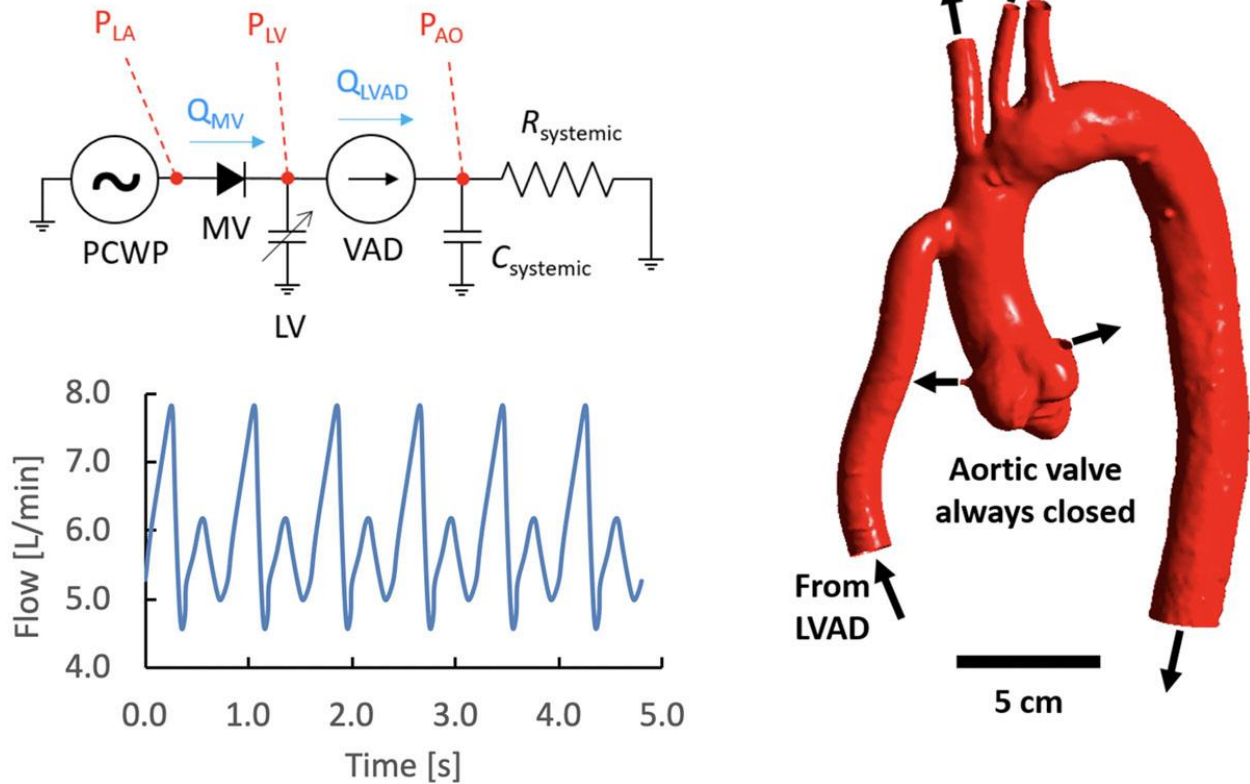


Figure 1 Computational model overview. Electric circuit (lumped parameter) model (top left), LVAD outflow waveform calculated from the model (bottom left) and 3D aortic anatomical model with LVAD outflow cannula (right). PCWP is Pulmonary wedge pressure; LA is left atrium; MV is mitral valve; LV is left ventricle; AO is aortic; VAD is ventricular assist device; R is resistance; C is capacitance.

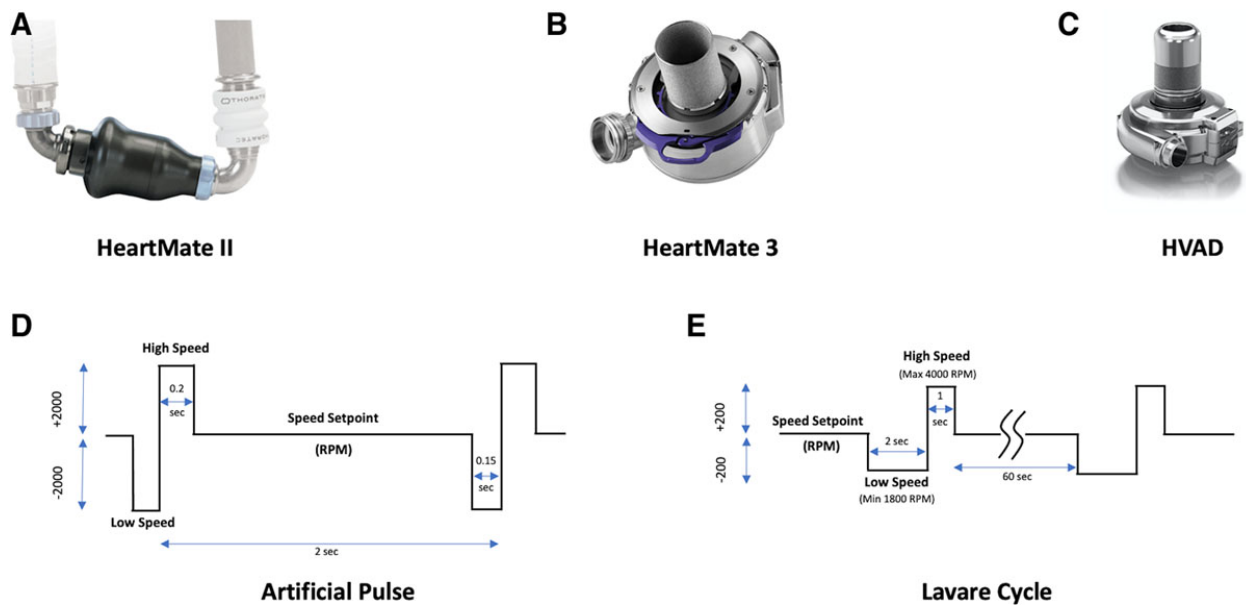


Figure 2 Ventricular assist devices that were incorporated in the model (A-C) and non-continuous operation modes of HM3 and HVAD (D-E). Images used with the permission of Abbott and Medtronic. Abbreviations as in figure 1.

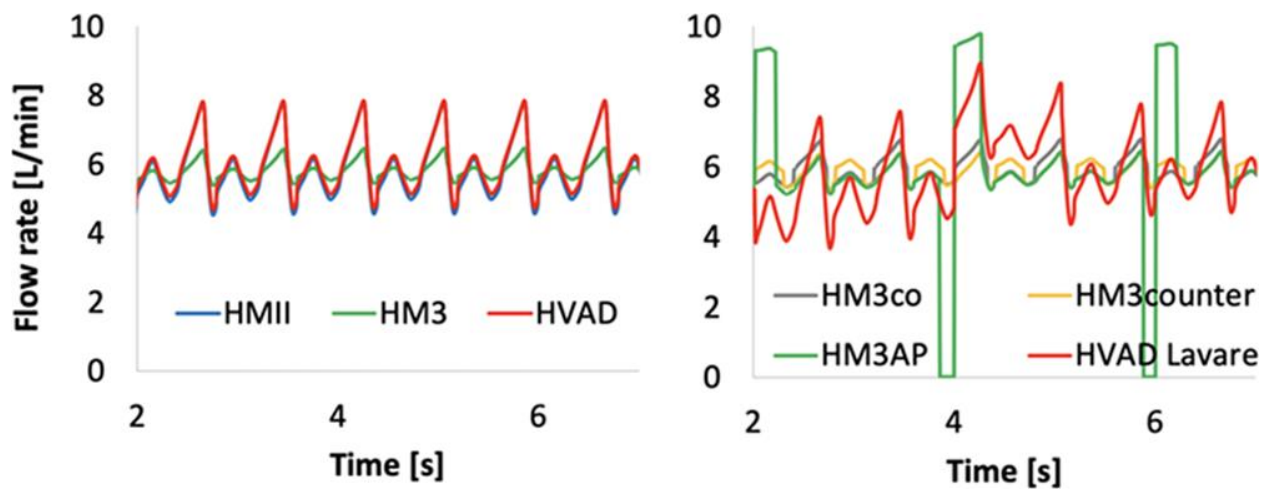


Figure 3 Predicted LVAD outflow waveforms: continuous modes (left) and non-continuous modes (right). Abbreviations as in figure 1.

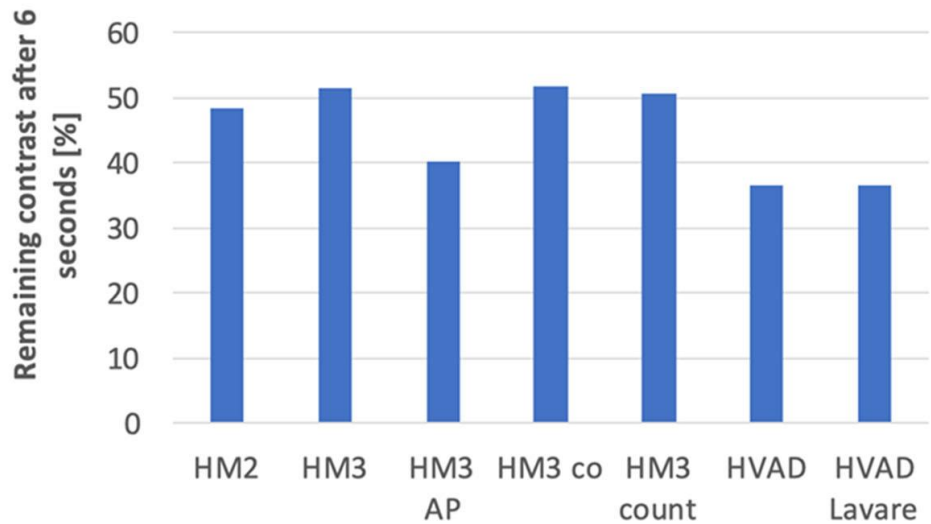
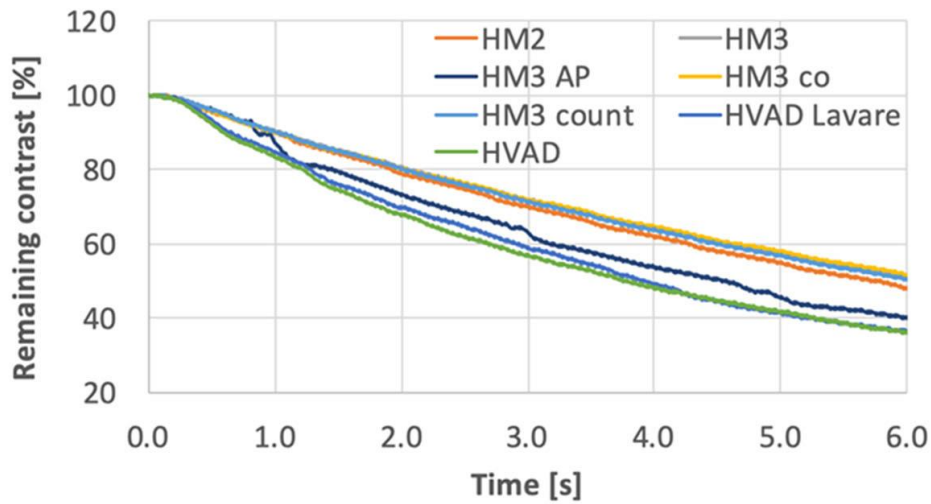
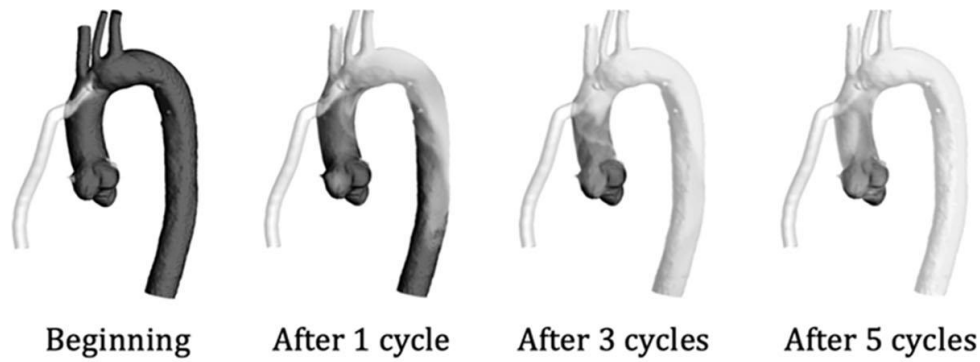


Figure 4 Virtual contrast agent flushing. Example of virtual contrast flushing from the aorta over time (top), time history of remaining contrast volume in the ascending aorta (middle) and remaining contrast volume in the ascending aorta after 6 seconds (bottom). Abbreviations as in figure 1; AP is artificial pulse; co is co-pulsation; count is counter-pulsation.

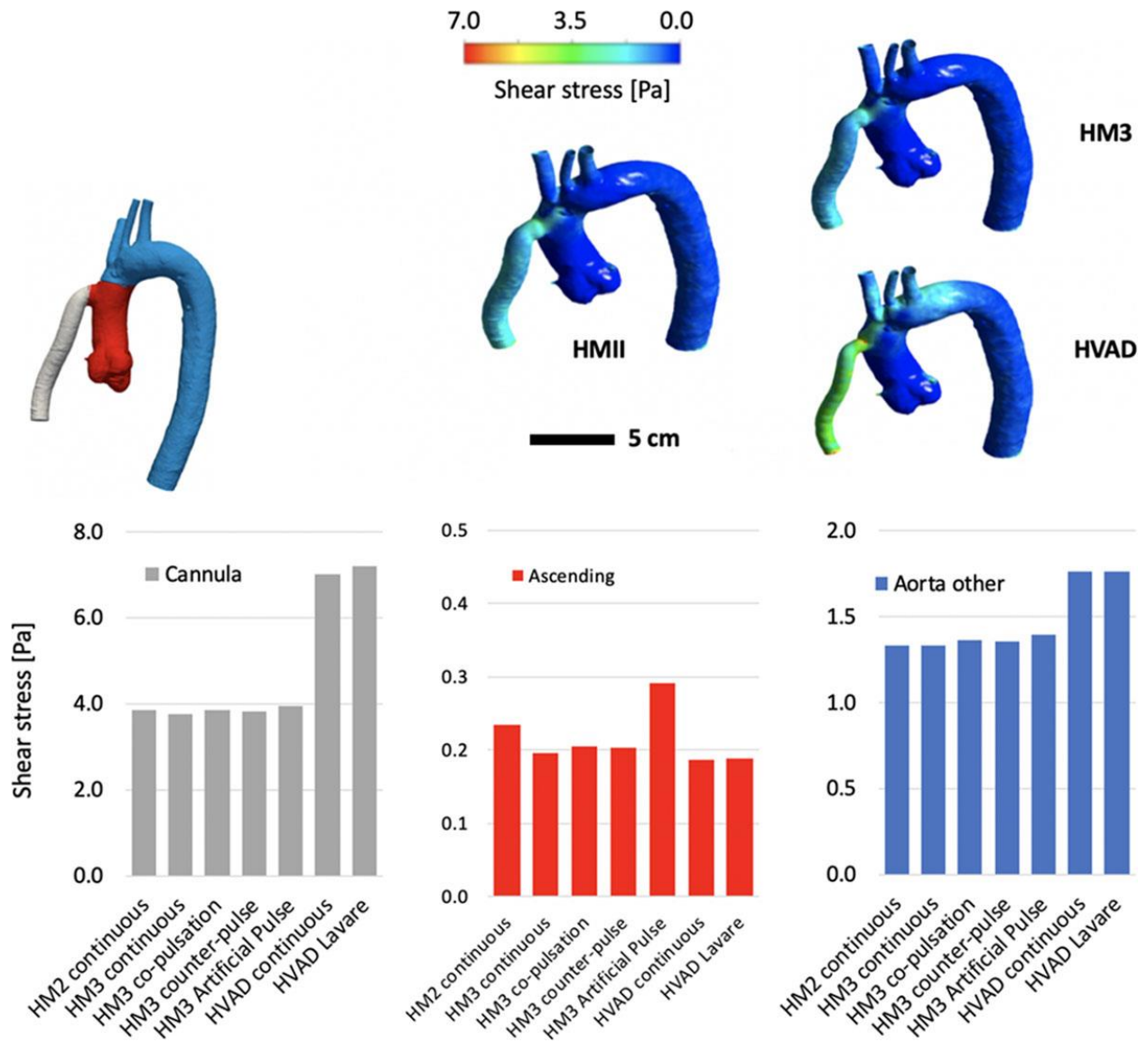


Figure 5 Wall shear stress quantification. Overall wall shear stress by LVAD type operating in continuous mode (top), wall shear stress by location (cannula, ascending aorta and the rest of the thoracic aorta) with and without programmable flow algorithms (bottom). Abbreviations as in figure 1.

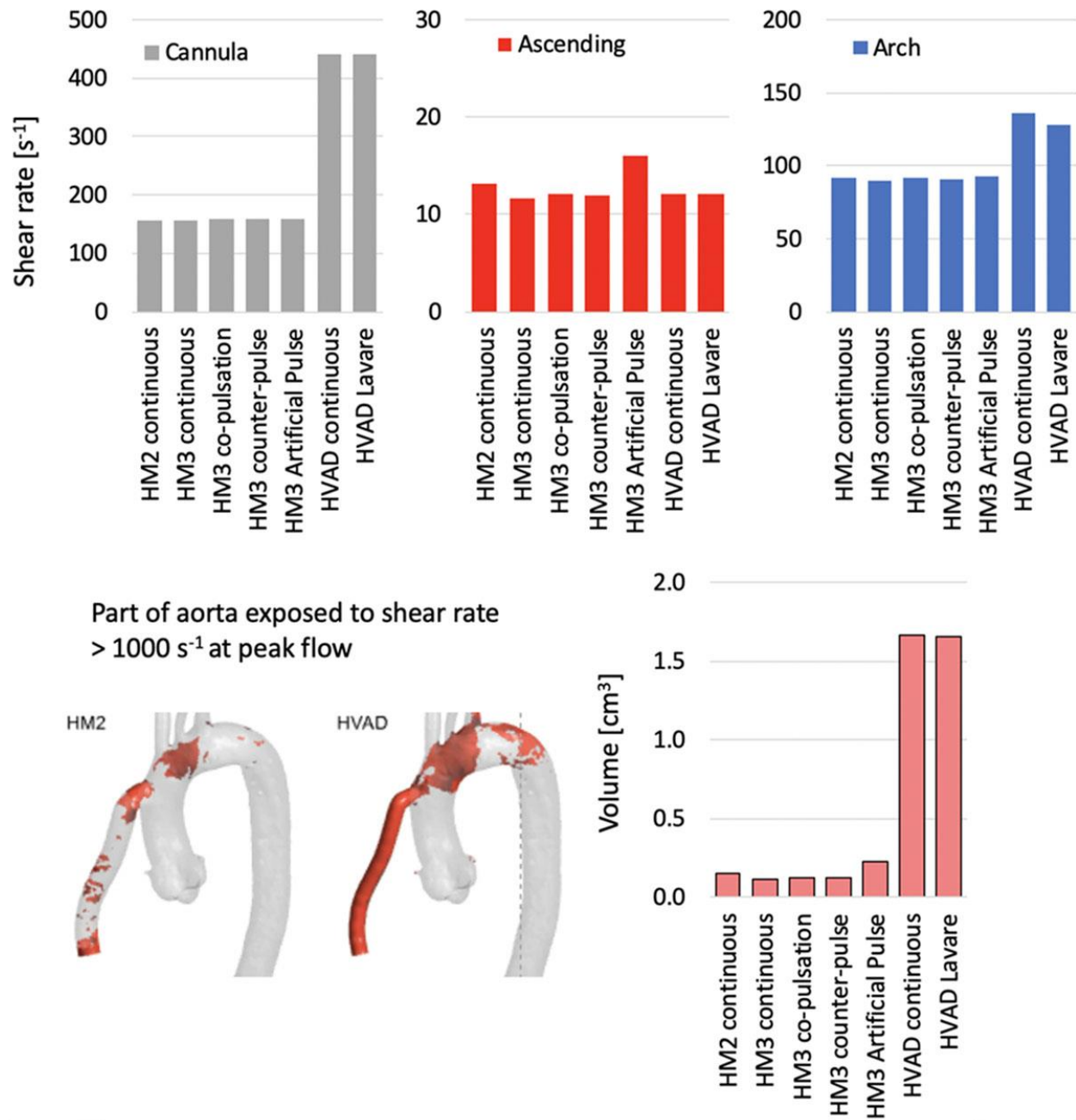


Figure 6 Quantification of shear rate in the blood stream. Shear rate by location (cannula, ascending aorta and the rest of the thoracic aorta) with and without programmable flow algorithms (top) and the volume exposed to high (> 1000 s⁻¹) shear rate (bottom). Abbreviations as in figure 1.